RESEARCH ARTICLE

WILEY

Parked aeroelastic field rotor response for a 20% scaled demonstrator of a 13-MW downwind turbine

Meghan Kaminski[1] [ORCID] | Eric Loth[1] | Lee Jay Fingersh[2] | Andy Scholbrock[2] | Michael Selig[3]

[1]Department of Mechanical and Aerospace Engineering, University of Virginia, Charlottesville, Virginia, USA

[2]National Renewable Energy Laboratory, Golden, Colorado, USA

[3]University of Illinois at Urbana-Champaign, Urbana, Illinois, USA

Correspondence
Meghan Kaminski, Department of Mechanical and Aerospace Engineering, University of Virginia, 122 Engineer's Way, Charlottesville, VA 22904, USA.
Email: mek3xc@virginia.edu

Abstract

Aeroelastic parked testing of a unique downwind two-bladed subscale rotor was completed to characterize the response of an extreme-scale 13-MW turbine in high-wind parked conditions. A 20% geometric scaling was used resulting in scaled 20-m-long blades, whose structural and stiffness properties were designed using aeroelastic scaling to replicate the nondimensional structural aeroelastic deflections and dynamics that would occur for a lightweight, downwind 13-MW rotor. The subscale rotor was mounted and field tested on the two-bladed Controls Advanced Research Turbine (CART2) at the National Renewable Energy Laboratory's Flatiron Campus (NREL FC). The parked testing of these highly flexible blades included both pitch-to-run and pitch-to-feather configurations with the blades in the horizontal braked orientation. The collected experimental data includes the unsteady flapwise root bending moments and tip deflections as a function of inflow wind conditions. The bending moments are based on strain gauges located in the root section, whereas the tip deflections are captured by a video camera on the hub of the turbine pointed toward the tip of the blade. The experimental results are compared against computational predictions generated by FAST, a wind turbine simulation software, for the subscale and full-scale models with consistent unsteady wind fields. FAST reasonably predicted the bending moments and deflections of the experimental data in terms of both the mean and standard deviations. These results demonstrate the efficacy of the first such aeroelastically scaled turbine test and demonstrate that a highly flexible lightweight downwind coned rotor can be designed to withstand extreme loads in parked conditions.

KEYWORDS
downwind, extreme-scale, field testing, flexible blades, gravo-aeroelastic scaling, parked, wind turbine

1 | INTRODUCTION

1.1 | Motivation for parked testing of rotors designed for extreme-scale turbines

Wind turbines are increasingly growing in height as well as blade length to increase the capture area thus increasing the maximum power available. This increase in blade length is coupled with an increase in flexibility is not seen in conventionally sized wind turbines.[1] Blade flexibility can limit upwind turbine sizes due to the increased potential of blade-tower strike, which arises from a combination of high thrust loads and turbulence-induced blade dynamics. One way to address this is to employ downwind turbines, which lessen the probability of a tower strike because thrust bends the blade away from the tower. In addition, downwind turbine designs provide load-aligned rotor blades to reduce the flapwise loads and corresponding structural requirements, creating lighter blades that can reduce the levelized cost of energy.[2] However, due to their lighter blades, downwind extreme-scale turbines (rated power in excess of 10 MW) need to consider extreme-wind speeds that may occur (e.g., hurricane conditions).[3] These loads occur primarily when the turbine is in a parked position and experiencing wind speeds significantly greater than the rated wind speed; therefore, design load cases (DLCs) for parked conditions are of utmost importance as design drivers for downwind extreme-scale turbines.[4] In some cases, parked conditions for an extreme-scale downwind turbine are the most important design drivers.[5]

Typically, modern turbine designs for parked conditions are based on simulations to ensure the turbine's ability to withstand extreme situations.[6,7] However, the accuracy of these predictions for the next generation of downwind extreme-scale turbines (which are likely to have highly flexible, coned, and complex geometry rotors) is not known. Experimental parked test data that are suitable for validation can facilitate better prediction and understanding of the dynamic loads on the blades and their unsteady aeroelastic responses.[8] Because the cost of testing a full-scale (e.g., for a 13-MW system) is extremely high, there is a strong motivation for developing subscale experimental demonstrators that are capable of capturing the same nondimensional behaviors as the full-scale turbine but at a fraction of the testing cost.[9–11]

1.2 | Previous scaled testing of wind turbines

There have been several previous subscale tests of wind turbines. For example, floating subscale turbines have been tested experimentally in parked situations, where scaling was used to replicate the influence of wave dynamics on the turbine and to evaluate the computational tools used for full-scale offshore turbine structures in unsteady sea-state conditions.[12,13] In particular, a 1/50th scale model of the National Renewable Energy Laboratory (NREL) 5-MW 126-m reference turbine[14] was tested in parked conditions.[12,14] This testing included hydrodynamic comparison of three distinct floating wind turbine concepts[12] in order to measure the entire wind turbine structural surge and pitch responses due to wave motion. Although this test achieved its objectives of understanding wind–wave–turbine interactions, there was no examination of the blade aeroelastic interactions (instead, the scaled rotor blades were designed to be rigid). Similarly, the VolturnUS turbine was tested (off the coast of Maine) using a 12.5% scaling of a 6-MW, 152-m-diameter turbine. The subscale turbine was designed based on Froude scaling to match the ratio of aerodynamic and wave loads during operation.[7,12,15] The hydrodynamic scale model was tested in a survival load case, with scaled conditions consistent with 500-year significant wave heights and mean associated wind speeds and currents.[12,13] Again, the primary objective was to measure the wind–wave interactions on the turbine response; the blade aeroelastic aspects were not considered.

Another example of subscale testing is NREL's Unsteady Aerodynamics Experiment (UAE) campaigns.[16] These tests assessed unsteady computational capabilities for stiff blades in stall conditions. Parked conditions were also considered, and the aerodynamic blade loads were studied.[4] The UAE employed rigid blades so the aeroelastic behavior is very different than what one would expect for an extreme-scale turbine, where the blades tend to be quite flexible.[17] To date, there has been no subscale parked testing that has sought to replicate the aeroelastic behavior of extreme-scale turbines (neither for upwind nor downwind rotor configurations). As a result, there has been no assessment of current computational capabilities for predicting blade deflections and loads in high gust conditions for flexible rotors.

To develop a methodology for designing subscale rotors, a gravo-aeroelastic scaling (GAS) method was developed for operational conditions in a nondimensional framework that replicates full-scale conditions.[18] This type of scaling considers geometry (including aerodynamic shapes and angles of attack), dynamics (such as blade frequencies relative to rotor rotation speed and nondimensional tip-speed ratios), and loads (gravitational, centrifugal, and aerodynamic forces and moments) to ensure that proper load angles, dynamics, and aeroelastic deflections of the blades are considered. The GAS concept has been theoretically proposed for operational conditions, for which it seeks to match the nondimensional turbine tip speed ratio, the ratio of rotor rotational speed and blade first flapping frequency, operational tip deflections (normalized by blade length), and blade moments (normalized by a combination of air density, rated wind speeds, and blade lengths).[18]

The theoretical operational scaling was recently used to scale the 100-m, 13.2-MW, Sandia National Laboratory's (SNL) upwind SNL 100–03 blade[19] down to a 1% scale blade model, and the scaling fidelity was investigated with ground testing.[18] More recently, GAS was used to design a 20% scaled blade to mimic the highly flexible, 104-m blade of the Segmented Ultralight Morphing Rotor (SUMR-13), a 13.2-MW downwind turbine blade with high flexibility and coning intended for offshore deployment. The SUMR-13 extreme-scale design indicates significant potential savings in the levelized cost of energy due to its lightweight, load-aligned design.[20–23] The 20% scale version of this rotor is termed the

SUMR-Demonstrator (SUMR-D), and parked conditions are analyzed herein. The scaled rotor blades were fabricated and installed at the NREL's Flatirons Campus (NREL FC) on the two-bladed Controls Advanced Research Turbine (CART2) testing tower and nacelle, which determined the scale of the blades.[9,10] The SUMR-D represents the largest downwind, highly flexible research wind turbine demonstrator designed and built in the United States in the last decade, and this study presents the first installed test results associated with this highly novel rotor design.

1.3 | Study objectives

The primary objective of the present study is to experimentally investigate the parked conditions of the SUMR-D turbine. To accomplish this, we tested the SUMR-D in horizontal parked conditions in both pitch-to-run and pitch-to-feather configurations for a large range of wind speeds at significant field-relevant turbulence levels. The data collected focused on unsteady flapwise loadings in the form of flapwise bending moments and aeroelastic blade deflections. We compared the results against the computational predictions, which used the structural digital twin of the SUMR-D turbine to investigate the capability of computational simulations to predict loading for this novel, flexible, downwind rotor with highly nonlinear aeroelastic behavior. In addition, we compared the results to the predicted full-scale SUMR-13 turbine response in order to assess the efficacy of the GAS method.

To our knowledge, this is the first study that experimentally and computationally investigates parked conditions using a gravo-aeroelastically scaled rotor. Additionally, this is the first parked test of a flexible downwind, two-bladed rotor using extreme-scale turbine design technology. It is also the first study to combine experimental and computational results to evaluate the efficacy of GAS for parked conditions and the first to evaluate computational predictive capabilities for blade deflections and loads in high gust conditions for a flexible rotor.

This study is organized as follows. Section 2 presents the experimental setup, data collection methods, scaling approach, and computational methods. Section 3 provides the experimental data and compares it to the FAST predictions of both the SUMR-D blade digital twin and the SUMR-13 blade in order to predict full-scale behavior. Finally, Section 4 provides conclusions and recommendations for further studies.

2 | METHODS: EXPERIMENTAL

2.1 | GAS

For radically new designs, such as the SUMR concept—which can exhibit highly nonlinear behavior—experimental testing is critical for proof of concept.[3] Because the full-scale design (SUMR-13) is a 13.2-MW system, full-scale testing is prohibitive from a cost perspective. Therefore, experimental testing of a scaled version (in this case, 20% scale) was employed. This degree of geometric scaling can reduce cost dramatically, when considering an all-new rotor system. In particular, a geometric scaling factor (η) that preserves nondimensional aeroelastic response generally results in a cubic change in rotor mass,[18] that is, the rotor mass of a subscale system will be proportional to η^3. As such, a 20% scaled system can roughly reduce manufacturing costs by a factor of 100 or more. Installation and testing costs can similarly be expected to be reduced by these great amounts. The present study sought to experimentally investigate the aeroelasticity of a 13-MW system, which includes a rotor blade length of 104.4 m. The most cost-effective and available test platform for a two-bladed rotor in the United States was the NREL CART2, which has a default blade length of 21.7 m for an upwind rotor, with minor coning. Placing a downwind highly coned rotor on this system required placing an adapter outboard of the pitch system, which allowed a blade length of 20.9 m. As such, the 20% subscale geometric ratio was based on available resources and cost-effective planning.

When employing geometric scaling for a new type of rotor to observe and understand the expected aeroelastic response, it is desirable to replicate the nondimensional aeroelastic behavior dynamics to the greatest degree possible. Replication of aeroelastic behavior is especially important because this novel design includes flexible blades in a downwind coned configuration. In particular, experimental testing would ideally replicate the nondimensional blade moments, deflections, and dynamics for the given aero-structural design. To this end, we designed and fabricated a subscaled demonstrator (SUMR-D) to replicate as closely as possible the nondimensional geometric, dynamic, and load-based aspects of the turbine within the constraints of the well-characterized, highly instrumented field test site.

For the present subscale rotor, the geometric scaling is based on the geometric ratio (η) of the blade length. For parked conditions, we focus on blade length as opposed to blade radius (blade length and hub radius) because the blade is nonrotating and therefore the hub radius does not affect the aerodynamic results. For the SUMR-D, η is based on 20% of the SUMR-13 design. This scaling is applied to all the critical aerodynamic dimensions. For example, the ratio of the scaled blade length (S_s) to the full-scale blade length (S_f) is set equal to η. Using this approach, the local spanwise positions along the blade length (s, where $s = 0$ is the blade root location) for both the subscale and full-scale rotors can be normalized as follows:

$$\overline{s} = s/S.$$

(1)

In this equation, the overbar (‾) denotes a nondimensional value. This same geometric scaling was then employed to ensure the same nondimensional blade chord length and airfoil thickness for both rotors as a function of the nondimensional blade length. In addition, the same airfoil shapes along both rotor blades were also employed.

Geometric angles between SUMR-D and SUMR-13 were maintained to the greatest degree possible by employing the same twist angle distribution along the nondimensional span, as well as the same angles of blade pitch, rotor coning, and blade azimuthal position. In particular, the current parked tests focused on braked conditions (for which rotor loads are highest) in the default T-position, with both blades parallel to the horizon. This fixed azimuthal configuration is a critical design load condition for two-bladed offshore wind turbines.[24]

In general, turbines are designed such that the rated and cut-out operating conditions are relative to average wind speeds. For the SUMR-13 design, the wind characteristics at hub height are based on Class IIB conditions using the International Electrotechnical Commission's IEC 61400 standards.[25] This yields an average wind speed of 8.5 m/s and a 50-year gust wind speed of 59.5 m/s. The cut-in, rated, and cut-out wind speeds for the SUMR-13 design were based on the NREL 5-MW (which is also a Class IIB turbine) wind speeds of 3, 11.3, and 25 m/s.[26] For a subscale system in operational conditions, the aerodynamic angles of attack and the ratio of thrust to centrifugal loads can be consistently maintained between the scale and full-scale systems by employing the same tip speed ratio and by scaling the wind speeds by $\eta^{1/2}$.[19] Because the SUMR-D was designed to have the same aeroelastic scaling for both parked and operational conditions, this $\eta^{1/2}$ scaling also applies to cut-out conditions and the 50-year gust. Therefore, the cut-in, rated, and cut-out wind speeds for an ideally scaled demonstrator are 1.34, 5.1, and 11.2 m/s, respectively, and the ideally scaled 50-year gust speed is 26.6 m/s. For ideal aeroelastic scaling, the SUMR-D should thus produce the same nondimensional deflections SUMR-13 at the same nondimensional wind speeds. For example, the tip deflection (δ_{tip}) is normalized by the blade length and the horizontal wind velocity upstream of the rotor (U_{horiz}) is normalized by the rated wind speed (U_{rated}). In addition, the nondimensional time is based on the ratio of the reference velocity and length scales. Based on the above, the nondimensional blade tip deflections, wind speeds, and time values are given as follows:

$$\overline{\delta}_{tip} = \delta_{tip}/S, \tag{2}$$

$$\overline{U}_{horiz} = U_{horiz}/U_{rated}, \tag{3}$$

$$\overline{t} = tU_{rated}/S. \tag{4}$$

To investigate the efficacy of this scaling, the nondimensional aeroelastic tip deflections of the scaled system ($\overline{\delta}_{tip,s}$) can be compared to that of the full-scale system ($\overline{\delta}_{tip,f}$) at the same nondimensional wind speed ($\overline{U}_{horiz}$).

This scaling can also be applied to the flapwise aerodynamic moments on the blade (M_{flap}). If one considers the parked blade in the pitch-to-run configuration, the blade is approximately perpendicular to the incoming flow, so the primary force is a drag force (as on a perpendicularly oriented flat plate).[27] Assuming the drag coefficient is independent for the SUMR-D and SUMR-13 system scales (a reasonable assumption given their high Reynolds numbers[27]), the steady force on such a blade is proportional to the surface area (which scales with η^2) and the dynamic pressure of the incoming wind ($\frac{1}{2}\rho_{wind}U_{horiz}^2$), where ρ_{wind} is the air density at hub height. The bending moments are proportional to blade length and this force; thus, the overall moment scaling is $\left(\frac{\rho_{wind,s}}{\rho_{wind,f}}\right)\eta^4$. As such, the nondimensional flapwise moment ($\overline{M}_{flap}$) for parked conditions can be defined as follows:

$$\overline{M}_{flap} = M_{flap}/\rho_{wind}U_{rated}^2 S^3. \tag{5}$$

This same scaling occurs for a pitch-to-feather configuration where lift forces dominate, as long as the angles of attack and the nondimensional blade geometry are consistent and as long as the lift coefficient curve does not vary significantly with the Reynolds number.

Another key parameter needed for aeroelastic scaling is the overall blade flexibility. Because the nondimensional tip deflection of a beam is proportional to the product of the moment applied and the beam length (normalized by the overall beam stiffness [EI]), the blade stiffness will scale with $\left(\frac{\rho_{wind,s}}{\rho_{wind,f}}\right)\eta^5$. This is because time scales as $\eta^{-1/2}$, based on Equation (4). Scaling the stiffness and frequency in this way for a simple beam with the same material density and structural design would result in the blade mass scaling as $\left(\frac{\rho_{wind,s}}{\rho_{wind,f}}\right)\eta^2$.[19] However, the stiffness varies greatly along the length of the blade for the SUMR-13 design (as is the case with most turbine blades); therefore, ensuring matched blade deflections also requires the nondimensional sectional stiffness (EI', stiffness per unit length) to be properly scaled, which should be nondimensionally preserved as a function of s/S, where

$$\overline{EI'} = EI'/\rho_{wind}gS^5. \tag{6}$$

For parked conditions, the blade stiffness can be based on zero velocity conditions (because there is no centrifugal blade stiffening). The geometry, velocity, time, moment, and stiffness scaling relationships developed here are listed in Table 1.

TABLE 1 Summary of select scaling factors for the GAS method

Scaling parameter	Scale factor
Length Scaling: $\frac{S_s}{S_f}$	η
Wind Velocity Scaling: $\frac{U_s}{U_f}$	$\sqrt{\eta}$
Distributed Blade Mass Scaling: $\frac{m'_s}{m'_f}$	$\left(\frac{\rho_{wind,s}}{\rho_{wind,f}}\right)\eta^2$
Stiffness Scaling: $\frac{(EI')_s}{(EI')_f}$	$\left(\frac{\rho_{wind,s}}{\rho_{wind,f}}\right)\eta^5$

FIGURE 1 The SUMR-D blades mounted on the two-bladed CART-2 at the NREL FC and placed in parked conditions

2.2 | Test facility and demonstrator turbine

As discussed above, the SUMR-13 was designed with a 104-m blade length and includes a morphing hinge at the root in order to reduce loadings during operation.[20,21,28–30] The SUMR-D is a 20% scaled model[9,10] designed to be tested on the CART2[31,32] at NREL FC. Parked conditions can generally include either idle conditions (the blade is free to rotate) or braked conditions (the blade is fixed at an azimuthal condition). Because braked conditions have the highest loads, which provide a more direct computational evaluation, only the braked conditions were employed in this study. Consistent with IEC design load suggestions, the braked conditions focused on the blades horizontal and parallel to the ground. Furthermore, although the blades are generally preferred to be in a pitch-to-feather configuration in parked conditions to reduce loads, the worst-case conditions (fault in the pitch controller, pitch-to-run configuration) should also be investigated as a design load case. Figure 1 shows the SUMR-D blades mounted on the CART2 tower at the NREL FC, with the blades parked in a horizontal T-position in a pitch-to-run configuration. The test included both pitch-to-run and pitch-to-feather configurations in the braked horizontal T-position.

As noted above, the full-scale SUMR-13 turbine is designed for Class IIB wind speeds. This is based on deployment in the Dominion offshore lease zone off the coast of Virginia, which prescribes a 50-year gust of 59.5 m/s and a turbulence intensity of 14%.[33] Based on the ideal wind scaling noted in Table 1, the aeroelastic design of the SUMR-D would be ideally tested at a site with a 50-year wind gust of 26.6 m/s and a

turbulence intensity of 14%. Furthermore, the scaled rated wind speed (using wind speed normalization per Equation 3) is 5.1 m/s and the scaled cut-out speed is 11.2 m/s. However, the subscale SUMR-D turbine was tested at the NREL FC. This site includes IEC Class IS (S: special) winds, which include 50-year gusts of ∼70 m/s and a turbulence intensity of 18%. A positive consequence of the higher wind speeds is that the NREL FC has a higher probability of wind speeds above the SUMR-D scaled cut-out wind speed (of 11.2 m/s), which helps in obtaining test data in high relative wind speeds for parked conditions.

However, the high wind speeds and turbulence levels of the NREL FC testing site are much more than an ideally scaled test site. This required the SUMR-D design to be much more structurally robust than would be dictated by ideal scaling (shown in Table 1). In particular, the inboard portion of the blade required extra structural mass. Figure 2 shows the nondimensional distributed blade stiffness with higher values at the root due to the extra structural mass, which resulted in a heavier blade than the ideally scaled blade (Table 2). However, the outboard section had a mass and stiffness distribution that was more consistent with the scaled values. Because the outboard portion stiffness is more important for blade deflection, this design compromise allowed aeroelastic scaling for the SUMR-D while ensuring safe deployment at the NREL FC.

Another constraint is the blade coning angle. The CART2 platform at the NREL FC contains an additional 3.7° shaft tilt (due to CART2 being primarily an upwind turbine) that is not present in the SUMR-13 design and the platform lacks the ability to accommodate a variable coning angle. To address these issues in the subscale rotor, a constant 12.5° coning angle adapter was attached at the root outboard of the pitch system. The coning adapter (located outboard of the pitch) was employed to avoid the high cost of changing the CART-2 pitch control mechanism for the field tests. Note that the full-scale system would be expected to be designed without such an adapter since the pitch would be activated outboard of
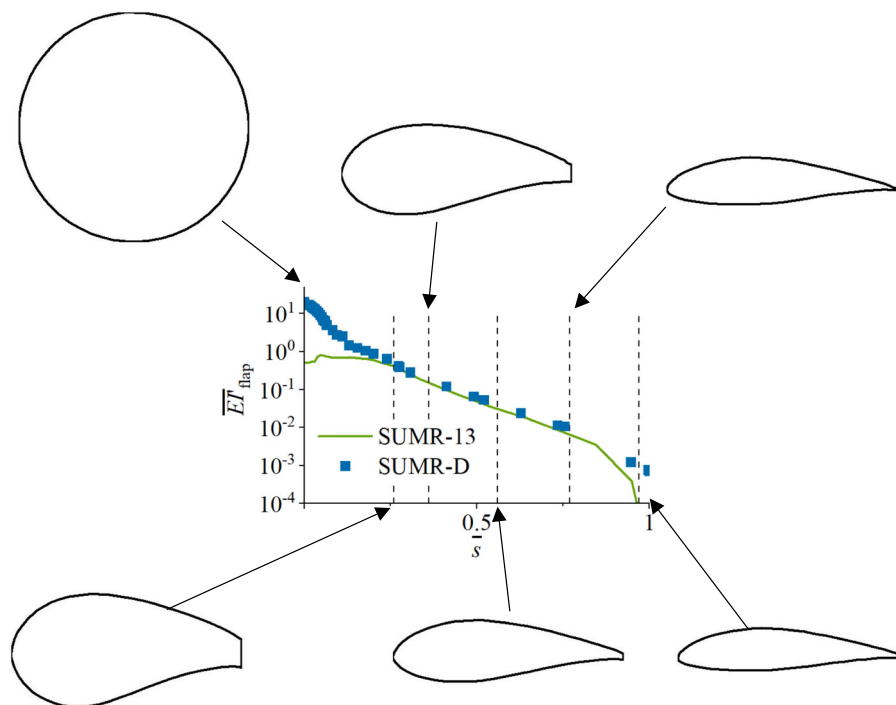
FIGURE 2 Nondimensional blade sectional stiffness ($\overline{EI'}$) as a function of the nondimensional span ($\overline{s}$) of the SUMR-13 and the 20% scaled SUMR-D; airfoil shapes (which were the same for both rotors) are also shown at select spanwise locations for the root (26%, 36%, 56%, 77%, and 97% span)

TABLE 2 Dimensional characteristics of the SUMR-D as fabricated and tested, the SUMR-D based on ideal aeroelastic scaling, and SUMR-13 as designed

|	SUMR-D	Ideal SUMR-D	SUMR-13
Blade length (S)	20.87 m	20.87 m	104.36 m
Rated velocity (U_{rated})	5.75 m/s	5.05 m/s	11.3 m/s
Cut-out velocity (U_{cut})	11.3 m/s	11.2 m/s	25 m/s
50-year gust ($U_{50-year}$)	∼70 m/s	26.6 m/s	59.5 m/s
Blade mass (m)	985.6 kg	350.6 kg	54,787 kg
Flapwise frequency	1.13 Hz	1.21 Hz	0.54 Hz

the coning). For these experiments in parked conditions, the net effect of this adapter was a change in the effective coning angle between the pitch-to-feather cases and the pitch-to-run cases. Because SUMR-13 was designed to be at a constant coning angle of 12.5° for operation in above-rated conditions, this ensured that the coning angle of SUMR-D was consistent with that of SUMR-13 in the worst-case condition of a pitch actuator fault and a pitch-to-run configuration. However, the use of an adapter outboard of the pitch control system resulted in a pitch-coning coupling as a function of pitch angle. In particular, 12.5° of coning ($\beta = 12.5°$) resulted when pitch to run ($\phi = 0°$), whereas 0° of coning ($\beta = 0°$) resulted when pitch to feather ($\phi = 90°$).

A summary of the differences in characteristics between the SUMR-13 turbine, an ideal scaled SUMR-D turbine, and the as-built SUMR-D turbine are listed in Table 2. The ideal SUMR-D values are based on the structure and environment of the full-scale SUMR-13 model with a 20% scaling factor applied. Due to the structural changes (as seen in Figure 2) made to account for the wind speed differences between the NREL FC and an ideal test site environment, the rated velocity was increased in order to maximize the tip deflections during operation to match the full-scale system.

2.3 | Measurement of wind characteristics

To compare tip deflections and root flap bending moments in parked conditions, we recorded detailed wind characteristics for the SUMR-D field tests at 400 Hz over each test interval. A typical test interval was about 5 min and 20 test intervals were used for total averaging. The wind speeds were read by the sonic anemometer on the meteorological tower, which is located 86 m upstream of the CART2 platform. The three components of the wind speed (in the x-, y-, and z-direction) were recorded at hub height. The x-direction was aligned with the primary wind direction pointing toward the CART2 turbine. Figure 3 shows the general layout of the CART2 platform operating as a downwind rotor, with the meteorological tower located 86 m upwind of the turbine from the predominant wind direction. The average wind shear was determined by averaging the gradient of the mean wind speed for a given test interval based on four cup anemometers distributed at 3, 15, 36.6, and 52.8 m above ground level on the meteorological tower as shown in Figure 3. Additionally, a cup anemometer was located on the hub of the rotor to determine instantaneous horizontal wind speeds (U_{horiz}) acting on the rotor plane.

We analyzed three data sets, one for each set of experimental results in the horizontal parked conditions: pitch-to-feather moments, pitch-to-run moments, and pitch-to-run deflections. Examples of horizontal wind speed data over 300-s intervals, drawn from the three data sets, are shown in Figure 4. The data sets were selected to ensure well-characterized inflow conditions. In particular, the data were chosen based on low cross-wind conditions (less than 2 m/s average cross winds) so that the average cross-wind angle for all data would be less than 10°. The data presented here were collected in October and November 2019, with the parked pitch-to-feather experiments taking place from November 16 to 18 and the pitch-to-run experiments taking place from October 11 to 22. The total analyzed lengths of data sets were 105 min (for the moments in the pitch-to-feather configuration), 105 min (for the moments in the pitch-to-run configuration), and about 100 min (for blade deflections).
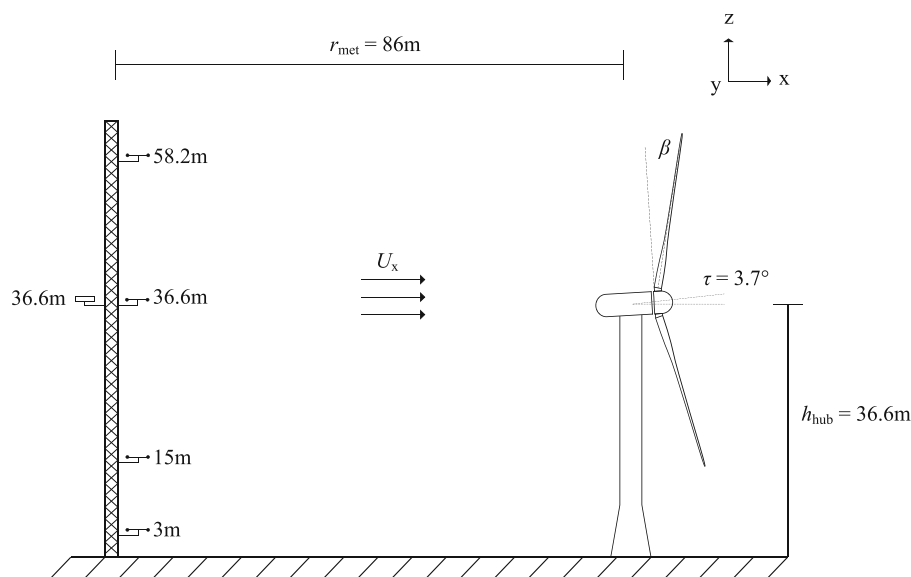
FIGURE 3 The CART2 tower with a 3.7° shaft tilt (τ) outfitted with the 20% scale SUMR blades and a variable coning angle (β) based on blade pitch. A meteorological tower is located 86-m upwind of the CART2 turbine, and it contains four distributed cup anemometers and a sonic anemometer at hub height

Table 3 provides a summary of each of these data sets and the average characteristics over the entire dataset. The cross-wind angle was computed using the meteorological tower U_x, U_y, and U_z wind speeds.

2.4 | Moments

The turbine root bending strain gauges are located 48 cm outboard from the root of Blade 1 of the SUMR-D rotor. The Blade 1 strain gauges for the flapwise and edgewise components are oriented based on a 0° pitch of the blade. The strain gauge output was converted into blade moments with the blades mounted on the turbine and compared to predicted root-bending moments. Due to the blades having higher mass than ideal, the low-wind gravitational moments were removed from the output bending moments in order to explicitly show aerodynamic results. Additionally, temperature drift caused the calibrations of the strain gauges to shift; therefore, to remove the gravitational moments in low wind speeds, a quadratic best fit of moment relative to wind speed (which assumes loads are proportional to the dynamic pressure) was applied to the data in 15-min increments to determine the zero-wind gravitational-only moments. This calibration approach minimizes the effects of temperature drift and allows the removal of the calibrated zero-wind bending moments. As such, the bending moments presented herein are due solely due to aeroelastic effects.

It should be noted that although the strain gauges are rated for a maximum of ±700 kN-m bending moments, the parked conditions rarely exceeded 10% of this limit. Typical operational values range from −100 to 100 kN-m. Combined with the aforementioned temperature drift and calibration, we estimate that the root-bending strain gauges are accurate to about 5% of the average values.

2.5 | Aeroelastic deflections

In order to obtain the aeroelastic blade deflections, we took optical measurements of the tip deflection. To accomplish this, a video camera was mounted on the hub and captured an image of the field of view toward the tip of the blade at 30 frames per second. The camera was aligned with the blade in the rotor azimuth direction but mounted inboard the pitch system, which meant that the pitch-coning coupling limited the effective camera field of view. In particular, the camera was mounted such that the blade was in frame while pitch to run (12.5° of coning), but out of frame while pitch to feather (0° of coning). The changing of frame angles is caused by the coning occurring outboard of the pitch system, as summarized in Section 2.2. Therefore, only deflections in the pitch-to-run configuration were obtained and presented.
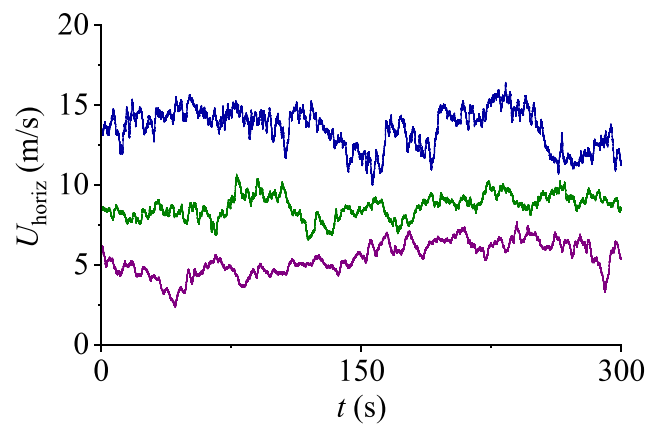
FIGURE 4 Three representative time variations of experimental wind speeds for the parked horizontal rotor configurations of the SUMR-D turbine taken over 5-min intervals, for a typical low (blue), medium (green), and high (pink) average wind

TABLE 3 Average wind characteristics of the SUMR-D parked experiments

	Total data length (min)	Sampling rate (Hz)	Mean velocity (m/s)	Mean turbulence intensity (%)	Mean ± StD crosswind angle (°)
Pitch to feather: moments	105	400	9.7	18.8	6.5 ± 16.9
Pitch to run:moments	105	400	13.4	22.6	−2.2 ± 22.4
Pitch to run: deflections	100	30	12.9	30.8	−9.7 ± 34.6

To analyze deflections due to aeroelastic effects, a reference state was used for the blade in a static, low-wind, horizontal pitch-to-run state. Tabs were mounted at 8 m, 13 m, and the tip of the blade, where these three tabs are denoted by their numerical subscripts. Figure 5(A) shows the reference image, which refers to the reference state using green arrows that point toward the three tabs located along the blade and their pixel locations ($p_{x,0}$ and $p_{y,0}$). The number of pixels for the three reference distances between a set of two tabs ($l_{tip-8,0}$, $l_{tip-13,0}$, $l_{13-8,0}$) are found in zero wind conditions (no aeroelastic deflection), and these distances define the reference blade shape. The set of three pixel distance values during parked testing (l_{tip-8}, l_{tip-13}, and l_{13-8}) for each frame of the desired video were found for each interval. Figure 5(B) shows an example of a frame during testing, with the green x-marks depicting the locations of each tab. To determine when an image corresponds to the reference frame (no net deflection), the root-mean-square error (L) of these values is determined as follows:

$$L = \sqrt{\left(l_{tip-8} - l_{tip-8,0}\right)^2 + \left(l_{tip-13} - l_{tip-13,0}\right)^2 + \left(l_{13-8} - l_{13-8,0}\right)^2}. \tag{7}$$

The frame of the desired video that minimizes this error is defined as the reference location for each tab. The subsequent pixel deflection distances for aeroelastic deflection for an interval were found relative to these values.

Photo by Lee Jay Fingersh, NREL.

Figure 5(A) is also used for the blade deflection pixel-to-distance calibration at the tip of the blade. This pixel-to-distance conversion for the tip of the blade was measured to be 3.17 mm/pixel. The total distance of deflections (δ_{tot}) is reported by converting the current frame's pixel distances from the zero location.

$$\delta_{tot} = \delta_{tip,pixel} \sqrt{\left(p_{tip,x} - p_{tip,x,0}\right)^2 + \left(p_{tip,y} - p_{tip,y,0}\right)^2} \tag{8}$$

Because the camera angle presents a singular two-dimensional plane of the blade, the deflection measured is based on a combination of bending or torsional deflection but does not include any out-of-plane bending that can occur, because the tabs are not located at the aeroelastic center of the blades. Such out-of-plane deflection is expected to be small, such that the deflection errors are less than 5% of the average values.

2.6 | Computational methods

We nondimensionally compared the experimental parked results to the computational SUMR-D and the computational SUMR-13 using FAST.[34] FAST is a wind turbine simulation software developed and maintained by NREL. The aerodynamic predictions employ two-dimensional airfoil results to evaluate three-dimensional rotor-blade performance. In order to accurately predict the three-dimensional results from the distributed airfoil results, a maximum drag coefficient for each of the airfoils is based on the average value from the experimental results, as outlined by Montgomerie.[35]
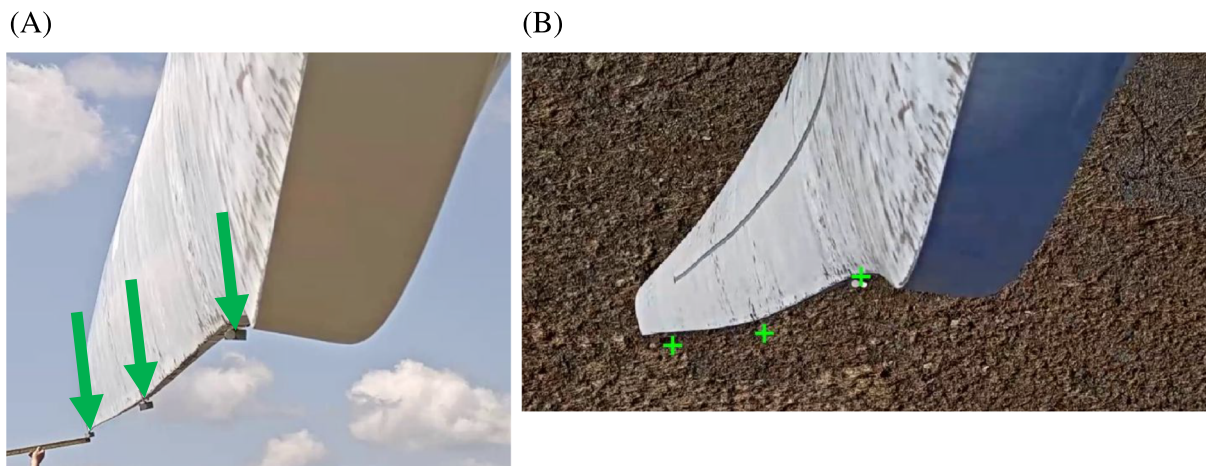
FIGURE 5 Tip deflection techniques showing (A) the pixel calibration and (B) a parked case with green plus (+) markers for all three tabs in the nondeflected state

The FAST simulations use TurbSim v2, a turbulence simulator for FAST, to create wind inputs designed to match the experimental wind field. These wind files are based on the sonic anemometer located on the meteorological tower and are used to define the time series, average horizontal flow angles, and average vertical flow angles. Additionally, the cup anemometers on the meteorological tower are used to determine the power law exponent of the wind profile to incorporate the effects of mean wind shear. Notably, TurbSim provides turbulence at the cross-sectional rotor plane that varies spatially and in time. As such, variations in the upstream turbulence and mean flow automatically occur along the length of the blade. Such variations also occur in the experimental field tests, but measurements were made at a single point far upstream in time so only the time variations were directly captured. The subscale wind input files were scaled such that the nondimensional turbulence seen at the rotor plane was matched between full-scale and subscale. An example of the horizontal velocity time series as measured and as used by FAST for SUMR-D and SUMR-13 is shown in Figure 6; this example is based on the nondimensional velocity and time variables using Equations (3) and (4). While there are differences in the time series for a given instant (e.g., at a nondimensional time of 45), the nondimensional average mean and the fluctuations about the mean for the simulations are consistent with experimental wind speeds. As such, one would expect mean and root-mean-square (rms) aeroelastic response to be similar if the aeroelastic structural scaling and aerodynamic were perfectly matched.

The SUMR-13 FAST structural and aerodynamic characteristics are based on computational designs.[20] The SUMR-D FAST structural characteristics employ a "digital twin" of the stiffness distribution (Figure 2), which was constructed based on the manufactured model, ground testing, and total mass down the length of the blade.[9] It can be seen that the SUMR-D blades have higher inboard stiffness than the SUMR-13 blades (due to NREL testing requirements). As such, one would expect greater mean and rms aeroelastic variations for SUMR-13 relative to SUMR-D. Moreover, there will be differences in aerodynamics between the subscale and full-scale systems due to Reynolds number effects, which can modify the lift and drag coefficients as a function of the angle of attack.

However, the differences in spanwise stiffness and aerodynamics between the experimental SUMR-D blades and the SUMR-D FAST blades would be expected to be small (since the latter uses a digital twin and the same Reynolds number). As such, one would expect similar spanwise mean and rms aeroelastic variations, were it not for the differences associated with unsteady aerodynamics (since the FAST aerodynamics assumes quasi-steady lift and drag with no vortex shedding and no hysteresis effects) and with the coning adapter (which could not be modeled within the FAST framework). The lack of this adaptor in the simulations is a limitation of the FAST code, whereby such geometry cannot be prescribed.

FAST was used to predict the edgewise and flapwise moments in the rotor reference frame as a function of time at a variety of stations along the blade length. To compare the predicted moments with those that were measured, a consistent reference frame was needed. The experimental moments are located at the 48-cm mark on the blade (2.3% of blade length) and are aligned with 0° pitch on the blade (this data does not consider blade twist). In comparison, FAST predicted moments taken about the point at 2.3% span are aligned with the local airfoil twist (φ) of 13.5° for the SUMR-13 blade and 34.3° for the SUMR-D blade (thus, these predictions do consider blade twist). To account for the differences in reference frames due to blade twist, the flap and edge moments predicted by FAST are rotated and aligned (to be consistent with the experimental flapwise moment coordinate frame) as follows:

$$M_{\text{flap}} = M_{\text{flap},\varphi} \cos\varphi - M_{\text{edge},\varphi} \sin\varphi, \tag{9}$$

To analyze the effects of aerodynamics and enable comparison to experimental data, each of the simulations is first run in zero-wind conditions for both pitch to run and pitch to feather to determine the moments due solely to gravity. These gravitational moments are then removed from the predicted moments, allowing only the effects of aeroelastic behavior on the blade bending moments to remain.
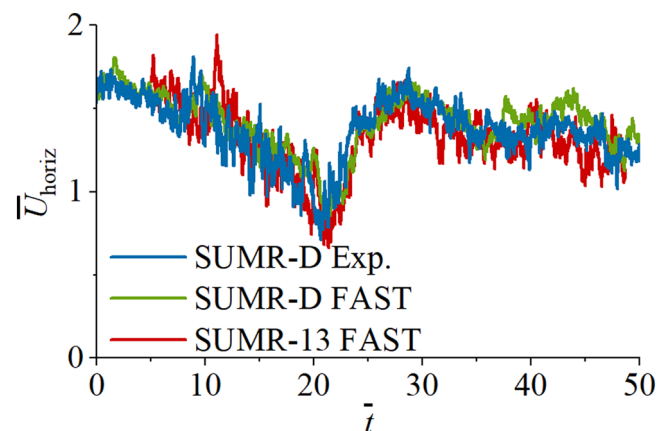
FIGURE 6 Example test interval of hub height, nondimensional horizontal wind speeds normalized by the rated wind speed as a function of nondimensional time. The speeds shown are from the SUMR-D experiments and the representative SUMR-D FAST and SUMR-13 FAST simulations

FAST also predicts both the edgewise and flapwise deflections separately. To compare these with the experimental total deflections, we combine the two predicted deflection distances as

$$\delta_{\text{tot}} = \sqrt{\delta_{\text{flap}}^2 + \delta_{\text{edge}}^2}. \tag{10}$$

As with moments, each simulation is run in zero-wind conditions for both pitch-to-feather and pitch-to-run configurations to obtain the deflections solely due to gravity. These effects are removed from the data to analyze the results of the aeroelastic behavior.

3 | RESULTS AND DISCUSSION

This section first considers the experimental results to show overall data trends and statistical convergence. Then, the experimental results are compared with the SUMR-D simulations to assess FAST predictive ability and to the SUMR-13 predictions to analyze the effectiveness of the GAS method. In all cases, the blades were in a horizontal position. Because FAST does not capture the effects of an adapter located outboard of the pitch actuator, a 12.5° of coning ($\beta = 12.5°$) was used in FAST when comparing with pitch-to-run conditions ($\phi = 0°$), and 0° of coning ($\beta = 0°$) was used in FAST when predicting the pitch-to-feather conditions ($\phi = 90°$).

3.1 | Experimental results

All the flapwise moment data are shown at the 2.3% span in the reference frame of the experimental strain gauges. For the parked experimental results, pitch-to-feather moments are presented in Figure 7, which shows the probability distribution function of the wind speeds in the data set
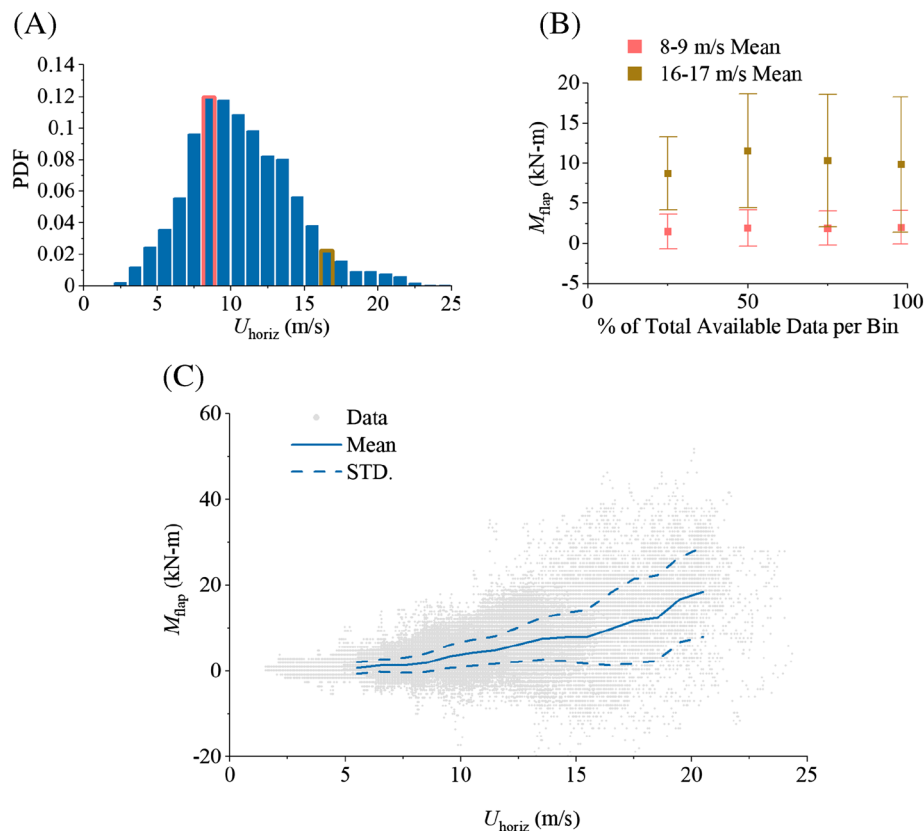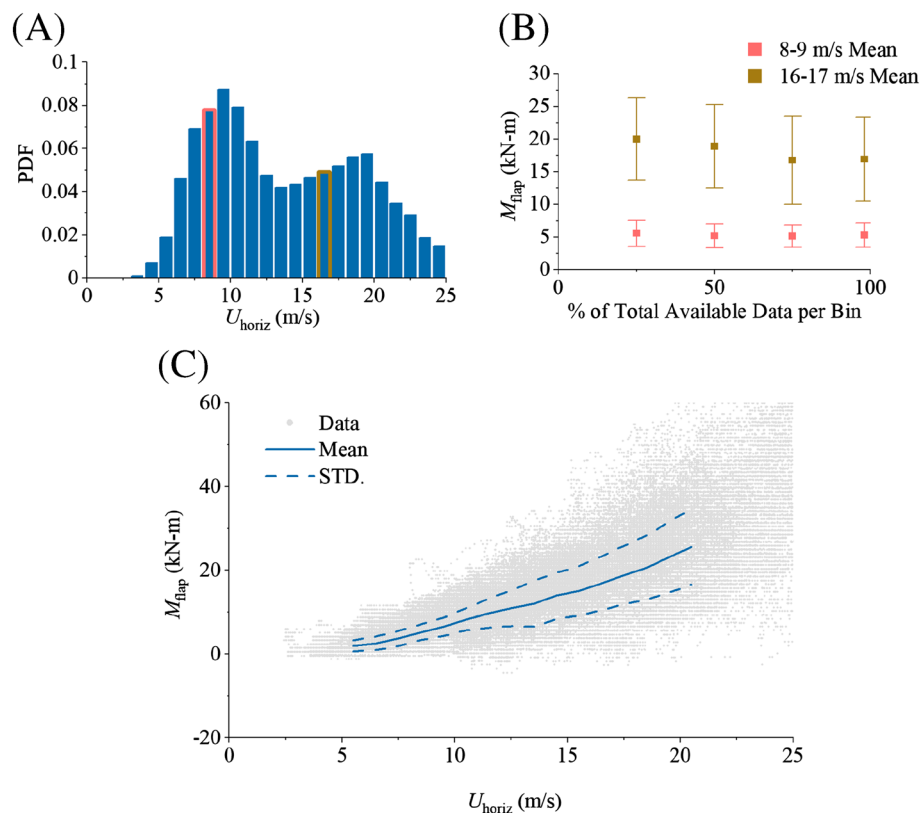

FIGURE 7 SUMR-D experimental horizontal pitch-to-feather moment simulations (105 min of data, sampled at 400 Hz) showing (A) the probability density of wind speeds, with bins used for the convergence analysis highlighted; (B) convergence analysis of the mean and standard deviations for two representative bins (8–9 and 16–17 m/s); and (C) the instantaneous nondimensional flapwise bending moments as a function of the nondimensional wind speeds along with the mean and ± one standard deviation, based on 1-m/s bins

based on 1-m/s bins. There is a significant amount of data above 11.2 m/s, the scaled cut-out wind speed of the SUMR-D rotor. This is due to testing at the NREL FC, where there is a high probability of high wind speeds.

Figure 7(B) shows the mean and one standard deviation of the flapwise moment for two sample bins (8–9 and 16–17 m/s) as a function of the percent of total available data per wind speed bin. The data show reasonable convergence over time; there are only small differences between the results for 75% vs. 100% of the total data collected. Using all data, Figure 7(C) shows the instantaneous flapwise bending moments as gray dots; the binned mean and standard deviations are shown as blue solid and dashed lines, respectively. Because the blade is in a pitch-to-feather configuration for this data, the positive slope is attributed to lift and increases quadratically with wind speed. This is expected because the blade loads scale with U_{horiz}^2. There are also large variations in the instantaneous moment about the mean, especially at high wind speeds. These variations can be attributed to the turbulence at the NREL FC and the influence of vertical velocity variations coupled with blade flexibility and dynamics, which combine to produce significant changes in the instantaneous angle of attack along the blade.

Using a similar analysis as in Figure 7, Figure 8 presents the flapwise bending moments for the experimental SUMR-D results in a pitch-to-run configuration. Figure 8(A) shows the distribution of wind speeds used for this study. Here, the data resulted in an even higher probability of high wind speeds, with as much as 50% of wind at speeds above the scaled cut-out speed of 11.2 m/s (for which the turbine is normally parked). Figure 8(B) again shows the convergence of average bending moments and their standard deviations, based on the percent of total data per bin. Again, the pitch-to-run moment data shows good convergence, with little change occurring between the 75% and 100% data sets. The wind and moment data are shown in Figure 8(C), with gray symbols indicating instantaneous pitch-to-run moments and blue solid and dashed lines, respectively, representing the mean and one standard deviation about the mean. With the blades in a pitch-to-run configuration, the increase in bending moments as a function of wind speeds is due to the increase in drag on the rotor. As expected, the means scale with U_{horiz}^2. The mean values for the pitch-to-run conditions are higher than those of the pitch to feather conditions, which is expected, as the drag on a blade that is perpendicular to the wind is higher than the lift when aligned with the wind. Again, there is a large variation in the instantaneous moment about the mean, which can be attributed to the turbulence at the NREL FC. In particular, the influence of streamwise velocity variations coupled with blade flexibility and dynamics combine to produce highly unsteady loadings.
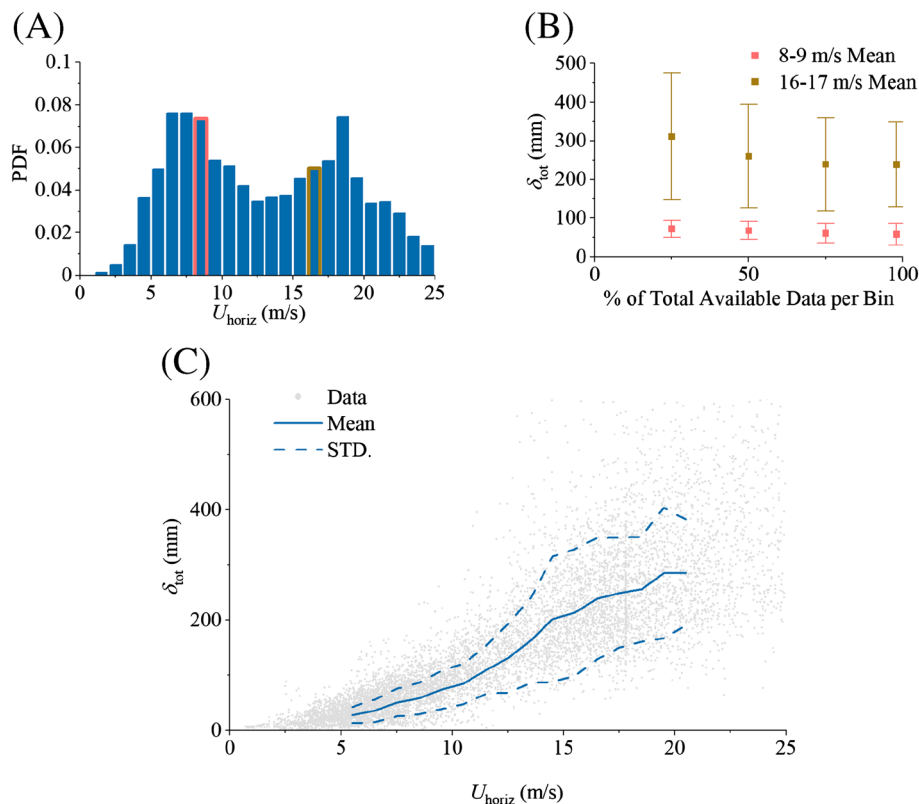

FIGURE 8 SUMR-D experimental horizontal pitch-to-run moment simulations (105 min of data, sampled at 400 Hz) showing (A) the probability density of wind speeds, with bins used for the convergence analysis highlighted; (B) a visualization of the convergence of the mean and standard deviations for two representative bins (8–9 m/s and 16–17 m/s); and (C) the distribution of nondimensional flapwise bending moments over nondimensional wind speeds along with the mean and ± one standard deviation

Next, Figure 9 presents the blade deflections for various wind speeds while the turbine is in a pitch-to-run configuration. Figure 9(B) shows the convergence of tip deflections. Again, there is substantial wind speed data above normal cut-out conditions, and reasonable convergence is demonstrated. This results in Figure 9(C), which shows the horizontal, parked, pitch-to-run deflections. Again, gray symbols indicate instantaneous deflections, while the solid and dashed blue lines represent the mean and one standard deviation about the mean, respectively. Similar to Figure 8 (C), the increase in tip deflections as a function of wind speeds is a result in an increase of drag on the blades and therefore scales with U_{horiz}^2. Again, there are large standard deviations, which increase as the wind speed increases. The aeroelastic deflections can reach 600 mm (3% of blade length) during these conditions. For a full-scale system, these deflections are consistent with deflections of 3.13 m in parked conditions. These results demonstrate that this highly flexible lightweight downwind coned rotor can withstand extreme loads in parked conditions. This was the primary objective of the field tests and points to the technical viability of such designs.

3.2 | SUMR-D FAST predictions

In order to assess the fidelity of FAST for predicting the moments and deflections of a coned downwind turbine with an advanced flatback airfoil design and highly flexible blades, we compared the SUMR-D experimental results with the SUMR-D FAST predictions with the same wind profiles. The FAST results are based on the same horizontal braked configuration as the experimental results and are subjected to similar non-dimensional wind speeds, as developed and summarized in Sections 2.3 and 2.6. For the following predictions and experiments, the data are again collected in 1-m/s bins.

Figure 10 presents the comparison of the SUMR-D experimental results against the SUMR-D FAST results for the parked, horizontal, pitch-to-run configurations. The solid lines represent the mean moments of each bin, and the shading and dashed lines represent the standard deviations about the mean. The results show good alignment between the experimental and computational data; the mean moments and standard deviations similarly increase as the wind speeds increase. There are some differences between the predictions and experiments. Some of this can

FIGURE 9 SUMR-D experimental horizontal pitch-to-run deflections simulations (100 min of data, sampled at 30 Hz) showing (A) the probability density of wind speeds, with bins used for the convergence analysis highlighted, (B) a visualization of the convergence of the mean and standard deviations for two representative bins (8–9 m/s and 16–17 m/s), and (C) the distribution of nondimensional flapwise bending moments over nondimensional wind speeds along with the mean and one standard deviation about the mean
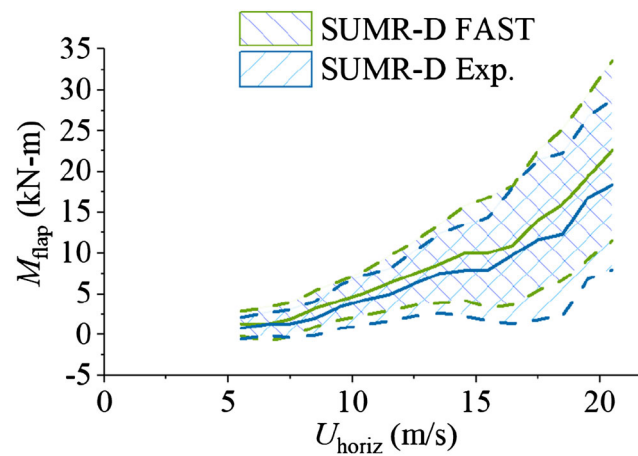
FIGURE 10   Comparison of SUMR-D experimental results with SUMR-D FAST results. The solid lines depict the mean bending moments for the bins, and the shaded regions and dashed lines depict ± one standard deviation in a horizontal pitch-to-feather configuration
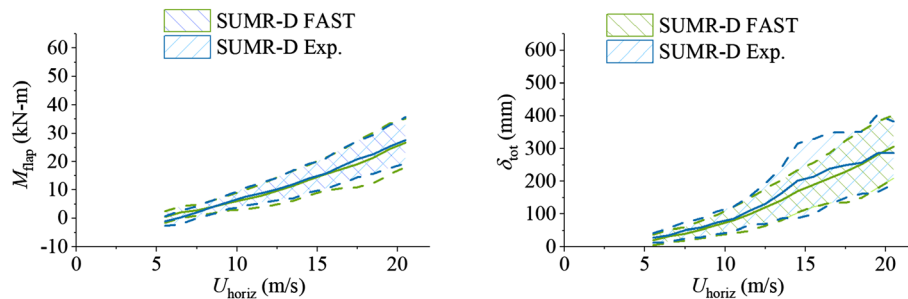
FIGURE 11   Comparison of SUMR-D experimental results with SUMR-D FAST results. The solid lines depict the mean values for each bin, and the shaded regions and dashed lines depict one standard deviation about the mean for (A) the flapwise bending moments and (B) the deflection distances in a horizontal pitch-to-run configuration

be attributed to insufficient statistical sampling, that is, the experimental results showed some dependence on the size of the experimental data sets (see Figures 8B and 9B). However, some of the differences can also be attributed to the limitations of the FAST computational framework. In general, the predictions tend to somewhat overpredict the experimental moments. For this pitch-to-feather configuration where the mean flow angle of attacks is relatively small but the relative variations driven by turbulence can be large, the differences can be attributed to an over-predicting of instantaneous lift coefficients, which is consistent with quasi-steady aerodynamic treatments of FAST. Despite this, the mean and standard deviations of the moments are reasonably replicated, which indicates that the wind flow input files for turbulence intensity and the models of the structural characteristics (especially blade stiffness) are allowing the unsteady fluctuations of the blade to be reasonably captured (nearly to within experimental uncertainty). Given the extremely high turbulence levels for these tests (see Table 3), and given the novel rotor design (downwind, coned, and high flexibility), this level of fidelity was not necessarily expected and indicates that FAST can reasonably predict the flapwise moments for parked conditions of a highly flexible lightweight downwind rotor (a secondary objective of the present study).

Figure 11 continues the comparison of experimental SUMR-D results to computational SUMR-D results by analyzing the horizontal, parked, pitch-to-run moments and deflections. In this configuration, the flow is nearly normal to the blade aerodynamic cross-section results in near-90° angles of attack. As such, flapwise bending moments are primarily due to airfoil drag associated with highly separated flow conditions (which can be very difficult to predict). For the FAST approach, sectional drag coefficients were specified based on previous blade drag measurements of three-dimensional (finite aspect ratio) blades at 90° angles of attack for the aerodynamic tests.[35] Based on these results and the current SUMR-D blade, a drag coefficient of 1.24 was specified at a 90° angle of attack with an empirical fit to map to other angles of attack above still conditions. This simple quasi-steady approach remarkably yields reasonable predictions of both the average bending moments and deflections in the pitch-to-run configurations as shown in Figure 11 (noting there is significant experimental uncertainty, especially for the deflection measurements). Additionally, the standard deviations are quite similar for the FAST and experimental values, suggesting that nonlinear effects of vortex shedding are not significant. Such a result is consistent with measured deflection dynamic frequencies, which indicated that the primary frequency of the

experimental tip deflection was related to low-frequency flapwise motion, related to the structural frequency of the blades (and not high-frequency chordwise vortex-induced vibrations). Overall, the results demonstrate that FAST is capable of predicting unsteady loads in high turbulence for high flexibility, downwind coned rotor design.

3.3 | Scaling assessment of demonstrator

Next, the experimental scaling method employed for this rotor is considered in terms of its ability to predict full-scale SUMR-13 performance. The computational SUMR-13 model is put in the same configuration as the experimental cases and is subjected to similar nondimensional wind speeds, as summarized in Sections 2.3 and 2.6. Additionally, the SUMR-13 results are binned in similarly scaled bin sizes as the experimental SUMR-D bins (1 m/s) by applying the wind speed scaling summarized in Section 2.1 for a SUMR-13 bin size of ∼2.23 m/s. Results are averaged in bin sizes in order to reduce uncertainties in results for a more accurate comparison.

For the parked, horizontal, pitch-to-feather conditions (with small angles of attack), Figure 12(A) and (B) present the nondimensional mean and standard deviations for the flapwise bending moments for the SUMR-D experimental, SUMR-D FAST, and SUMR-13 FAST results. For cases, the mean moments and the rms of their fluctuations increase at higher wind speeds due to increased loads and fluctuations (which scale with the square of wind speed). The predicted and measured mean moments for SUMR-D show reasonable alignment through the range of wind speeds for the pitch-to-feather configuration. Again, this indicates appropriate coefficients of lift for the subscale system, and it additionally indicates minimal effects of Reynolds number differences on the coefficient of lift (at least for parked condition response). Figure 12(B) shows the standard deviations of each rotor with the SUMR-13 turbine exhibiting higher standard deviations than the SUMR-D rotors (simulated and experimental). This expected difference is attributed to the higher nondimensional distributed stiffness of the SUMR-D-manufactured blades (required for NREL FC site testing) as shown in Figure 2, relative to that for the SUMR-13 full-scale system. Higher stiffness for the SUMR-D blades lends itself to higher restoring forces against fluctuations in the wind, causing smaller blade fluctuations during turbulent conditions. However, the overall response shows that the aeroelastic scaling approach can allow subscale system experimental testing that is reflective of full-scale system response and that FAST can capture the physics of the blade response in highly turbulent parked conditions. The much lower costs associated with building and testing a 20% scale turbine compared to a full-scale turbine indicate the enormous cost-effectiveness of subscale testing in validating novel extreme-scale turbines.

Similar results are seen in Figure 13 for the horizontal, pitch-to-run configurations. Figure 13(A) shows reasonably accurate results of the mean flapwise bending moments for the FAST simulations. The simulations use airfoils with a maximum coefficient of drag of 1.24. Figure 13(B) presents the standard deviations of the rotor over the range of wind speeds. Similar to the pitch-to-feather conditions, FAST shows higher mean and fluctuating moments for the SUMR-13 than for the SUMR-D, which are expected and attributed to higher blade stiffness in the subscale model (Figure 2).

Finally, Figure 14 shows the deflection distances of a parked, horizontal, pitch-to-run configuration. Figure 14(A) and 14(A) present results similar to those seen in Figure 13; however, the deflections have higher differences due to their additional sensitivity to bending stiffness. As expected, FAST predicts higher mean and fluctuating deflections for the SUMR-13 simulations than those of the SUMR-D blades due to the higher stiffness of the SUMR-D blades (Figure 2), which then alters their beam restoring forces. It should also be noted that the experimental SUMR-D deflections are higher than the predicted values at a velocity ratio of 2.5. This may be due to experimental uncertainty and also due to the nonlinear behavior of the blade structural dynamics or aerodynamics (e.g., vortex-induced oscillations) not captured by the FAST framework. However, the overall response demonstrates that subscale experimental testing can be used to provide experimental results that are reflective of the full-scale design of novel extreme-scale turbines and that the FAST framework can capture the key trends.
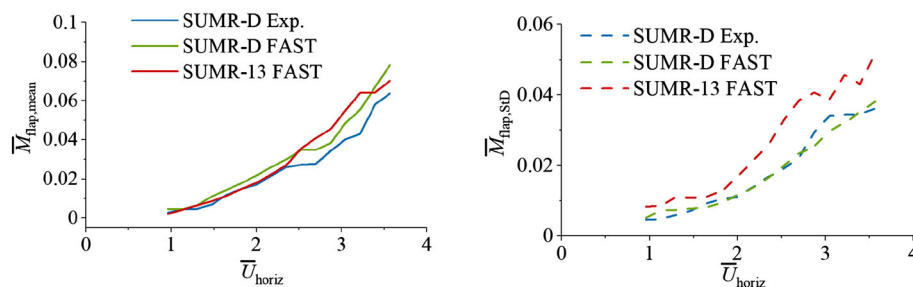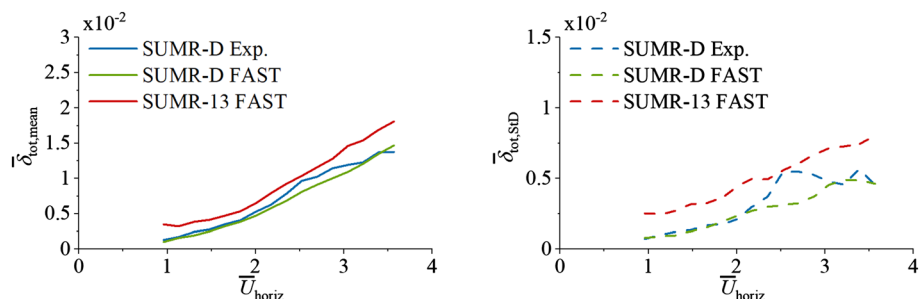

FIGURE 12 A nondimensional comparison of the SUMR-D experimental data, SUMR-D FAST data, and SUMR-13 FAST data showing (A) the means and (B) the standard deviations of the horizontal pitch-to-feather bending moments
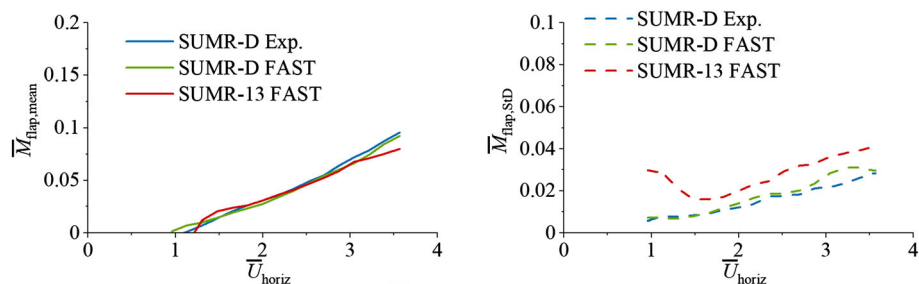
FIGURE 13 A nondimensional comparison of the SUMR-D experimental data, SUMR-D FAST, and SUMR-13 FAST showing (A) the means and (B) the standard deviations of the horizontal pitch-to-run bending moments

FIGURE 14 A nondimensional comparison of the SUMR-D experimental data, SUMR-D FAST, and SUMR-13 FAST showing (A) the means and (B) the standard deviations of the horizontal pitch-to-run deflection distances

4 | CONCLUSIONS AND RECOMMENDATIONS

This study presents time-dependent parked testing results of a gravo-aeroelastically scaled 20.9-m subscale blade model to represent the 104.4-m SUMR-13 blade. The subscale blades were designed for mounting on the CART2 turbine and were operated in a downwind configuration at the NREL FC. Due to the NREL FC having higher than ideally scaled wind speeds and turbulence, the demonstrator blades were designed and manufactured to have higher nondimensional mass and stiffness values as compared to the full-scale model. However, this had the benefit of considering the rotors in extreme conditions, which is critical for robust design. The parked testing results presented were performed in the braked horizontal pitch-to-feather and pitch-to-run configurations for unsteady flapwise bending moments for a range of binned wind speeds. In addition, unsteady aeroelastic deflections were also measured for the pitch-to-run configuration.

The experimental results were compared against computational results for both the full-scale SUMR-13 and the "digital twin" of the SUMR-D rotor. The computational results utilized FAST using input wind speed files from TurbSim v2 to reflect the experimental wind field. The results of SUMR-D FAST indicated that the predicted three-dimensional lift and drag coefficients provide a high-fidelity representation of the aerodynamic loads despite the complex coned geometry and high flexibility of the blades. The FAST results are encouraging to the authors as a valuable source for predicting the experimental blade dynamics. Additionally, the nondimensional results aligned well with the full-scale SUMR-13 rotor, once the blade stiffness adjustments (needed to withstand the extreme wind conditions at the NREL FC) were considered. The results also show that tip deflections at high wind speeds are reasonable. This demonstrates the SUMR-13 concept (for which there was no previous experimental data) is a feasible design in terms of handling parked conditions for the extreme case of a braked setting with both pitch-to-feather and pitch-to-run configurations. This supports the viability of a downwind, lightweight, flexible rotor concept for extreme-scale turbines. Importantly, the present experimental and computational results show that the aeroelastic scaling approach proposed herein allows subscale experimental testing that is highly reflective of full-scale design response. This scaling can be an enormous cost advantage for validating novel extreme-scale turbines. We recommended that this study be continued in order to analyze the operational conditions and further understand the efficacy of the FAST simulations, as well as to further analyze and develop the GAS method.

PEER REVIEW

The peer review history for this article is available at https://publons.com/publon/10.1002/we.2794.

DATA AVAILABILITY STATEMENT

Raw data supporting the findings of this study are stored by NREL and are available from the corresponding author upon request.

NOMENCLATURE

EI	blade stiffness
h	height
g	gravitational constant
L	root-mean-square error of deflections
l	distance between tabs
m	blade mass
M	moment
P	applied load
p	pixel
r	distance
s	spanwise location
S	total blade length
t	time
U	wind speed
β	variable cone angle
δ	deflection
η	scaling factor
ρ	density
ϕ	blade pitch
φ	local airfoil twist angle
τ	shaft tilt

SUBSCRIPTS

$()_0$	reference value
$()_{50-year}$	50-year gust
$()_{cut-out}$	cut-out value
$()_{edge}$	edgewise value
$()_f$	full-scale value
$()_{flap}$	flapwise value
$()_{hub}$	hub value
$()_{horiz}$	horizontal value
$()_{met}$	meteorological tower value
$()_{pixel}$	pixel-to-distance conversion
$()_{rated}$	rated value
$()_s$	subscale value
$()_{tip}$	tip location
$()_{tot}$	distance value
$()_{wind}$	wind value
$()_{xx}$	spanwise location
$()_{x,y,z}$	coordinate frame
$()'$	spanwise distributed value
$\overline{()}$	nondimensional value

ORCID

Meghan Kaminski https://orcid.org/0000-0003-2233-4784

REFERENCES

1. Bir G, Jonkman JM. Aeroelastic instabilities of large offshore and onshore wind Turbinesa. *J Phys E*. 2007;75:012069. doi:10.1088/1742-6596/75/1/012069

2. Zalkind DS, Ananda GK, Chetan M, et al. System-level design studies for large rotors. *Wind Energy Sci Discuss*. 2019;4(4):595-618. doi:10.5194/wes-2018-80

3. Li Z, Wen B, Dong X, Peng Z, Qu Y, Zhang W. Aerodynamic and aeroelastic characteristics of flexible wind turbine blades under periodic unsteady inflows. *J Wind Eng Ind Aerodyn*. 197:104057. doi:10.1016/j.jweia.2019.104057

4. Madsen PH, Pierce K, Buhl M. Predicting ultimate loads for wind turbine design work performed under task number WE903330. 1999. doi: NREL/CP-500-25787.

5. Goude A, Rossander M. Force measurements on a VAWT blade in parked conditions. *Energies*. 2017;10(12):1954. doi:10.3390/en10121954

6. Cotrell J. *The mechanical design, analysis, and testing of a two-bladed wind turbine hub*. 1993. doi: NREL/TP-500-26645

7. Dagher H, Viselli A, Goupee A, Kimball R, Allen C. The VolturnUS 1:8 Floating wind turbine: design, construction, deployment, testing, retrieval, and inspection of the first grid-connected offshore wind turbine in US. doi: DE-EE0003278.001.

8. Osgood R, Bir G, Mutha H, Peeters B, Luczak M, Sablon G. Full-scale modal wind turbine tests: comparing shaker excitation with wind excitation. in IMAC-XXVII (Society for Experimental Mechanics, 2010).

9. Yao S, Griffith DT, Chetan M, et al. A gravo-aeroelastically scaled wind turbine rotor at field-prototype scale with strict structural requirements. *Renew Energy*. 2020;156:535-547. doi:10.1016/j.renene.2020.03.157

10. Bay CJ, Damiani R, Fingersh LJ, et al. Design and testing of a scaled demonstrator turbine at the National Wind Technology Center. AIAA Scitech Forum. 2019. doi: NREL/CP-5000-72658.

11. Bottasso CL, Campagnolo F, Petrović V. Wind tunnel testing of scaled wind turbine models: beyond aerodynamics. *J Wind Eng Ind Aerodyn*. 2014;127:11-28. doi:10.1016/j.jweia.2014.01.009

12. Goupee AJ, Koo BJ, Kimball RW, Lambrakos KF, Dagher HJ. Experimental comparison of three floating wind turbine concepts. *J Offshore Mech Arct Eng*. 2014;136(2):020906. doi:10.1115/1.4025804

13. Viselli AM, Goupee AJ, Dagher HJ. Model test of a 1:8-scale floating wind turbine offshore in the Gulf of Maine. *J Offshore Mech Arct Eng*. 2015;137(4):041901. doi:10.1115/1.4030381

14. Martin HR, Kimball RW, Viselli AM, Goupee AJ. Methodology for wind/wave basin testing of floating offshore wind turbines. *J Offshore Mech Arct Eng*. 2014;136(2):021902. doi:10.1115/1.4025030

15. Viselli AM, Goupee AJ, Dagher HJ, Allen C. Design and model confirmation of the intermediate scale VolturnUS floating wind turbine subjected to its extreme design conditions offshore Maine. *Wind Energy*. 2016;19:1161-1177.

16. Simms DA, Hand MM, Fingersh LJ, Jager DW. Unsteady aerodynamics experiment phases II-IV test configurations and available data campaigns. 1999. doi: NREL/TP-500-25950.

17. Noyes C, Qin C, Loth E. Tower shadow induced blade loads for an extreme-scale downwind turbine. *Wind Energy*. 2020;23(3):458-470. doi:10.1002/we.2415

18. Kaminski M, Loth E, Griffith DT, Qin C. Ground testing of a 1% gravo-aeroelastically scaled additively-manufactured wind turbine blade with bio-inspired structural design. *J Renew Energy*. 2020;148:639-650. doi:10.1016/j.renene.2019.10.152

19. Griffith DT, Richards PW. *The SNL100–03 blade: design studies with flatback airfoils for the Sandia 100-meter blade*. 2014. doi: SAND2014–18129.

20. Ananda GK, Bansal S, Selig MS. Aerodynamic design of the 13.2 MW SUMR-13i wind turbine rotor. *AIAA SciTech Forum* (2018). doi:10.2514/6.2018-0994

21. Noyes C, Qin C, Loth E. Pre-aligned downwind rotor for a 13.2 MW wind turbine. *Renew Energy*. 2018;116:749-754. doi:10.1016/j.renene.2017.10.019

22. Ichter B, Steele A, Loth E, Moriarty P, Selig MS. A morphing downwind-aligned rotor concept based on a 13-MW wind turbine. *Wind Energy*. 2016;19(4):625-637. doi:10.1002/we.1855

23. Loth E, Steele A, Qin C, Ichter B, Selig MS, Moriarty P. Downwind pre-aligned rotors for extreme-scale wind turbines. *Wind Energy*. 2017;20:1241-1259.

24. Kim T, Larsen TJ, Yde A. Investigation of potential extreme load reduction for a two-bladed upwind turbine with partial pitch. *Wind Energy*. 2015;18(8):1403-1419. doi:10.1002/we.1766

25. International Eletrotechnical Commission. IEC 61400-1 wind turbines—part 1: design requirements. *Wind turbines – Part 1 Des. Requir* 2005. 2005:1–92.

26. Jonkman JM, Butterfield S, Musial W, Scott G. Definition of a 5-MW reference wind turbine for offshore system development. Contract. 2009. doi: NREL/TP-500-38060.

27. Igarashi T, Terachi N. Drag reduction of flat plate normal to airstream by flow control using a rod. *J Wind Eng Ind Aerodyn*. 2002;90(4-5):359-376. doi:10.1016/S0167-6105(01)00198-2

28. Loth E, Selig MS, Moriarty P. Morphing segmented wind turbine concept. AIAA Appl Aerodyn Conf 1–6. 2010. doi:10.2514/6.2010-4400

29. Loth E, Steele A, Ichter B, Selig MS, Moriarty P. Segmented ultralight pre-aligned rotor for extreme-scale wind turbines. in AIAA Aerospace Sciences Meeting. 2012. doi:10.2514/6.2012-1290

30. Noyes C, Qin C, Loth E. Ultralight, morphing rotor for extreme-scale wind turbines. in AIAA SciTech Forum. 2017. doi:10.2514/6.2017-0924

31. Bossanyi EA, Wright AD, Fleming PA. Controller field tests on the NREL CART2 turbine. 2010. doi: NREL/TP-5000-49085

32. Stol KA. Geometry and structural properties for the controls advanced research turbine (CART) from model tuning. Nrel/Sr 500–32087. 2004. doi: NREL/SR-500-32087.

33. Virginia offshore 90-meter wind map and wind resource potential. Available at: https://windexchange.energy.gov/maps-data/237. (Accessed: 9th December 2019).

34. Jonkman JM, Buhl ML. FAST user's guide. 2005. doi: NREL-EL-500-38230.

35. Montgomerie B. *Drag coefficient distribution on a wing at 90 degrees to the wind*. 1996. doi: ECN-C--95-061.